International Journal of Geo-Information

MDPI

Article

Mapping and Quantification of the Dwarf Eelgrass *Zostera noltei* Using a Random Forest Algorithm on a SPOT 7 Satellite Image

Salma Benmokhtar [1,2,*], Marc Robin [2], Mohamed Maanan [2] and Hocein Bazairi [1]

[1] BioBio Research Center, BioEcoGen Laboratory, Faculty of Sciences, Mohammed V University in Rabat, Rabat 1014, Morocco; hocein.bazairi@um5.ac.ma
[2] LETG UMR CNRS 6554, University of Nantes, CEDEX 3, 44312 Nantes, France; marc.robin@univ-nantes.fr (M.R.); mohamed.maanan@univ-nantes.fr (M.M.)
* Correspondence: salma_benmokhtar@um5.ac.ma

Abstract: The dwarf eelgrass *Zostera noltei* Hornemann (*Z. noltei*) is the most dominant seagrass in semi-enclosed coastal systems of the Atlantic coast of Morocco. The species is experiencing a worldwide decline and monitoring the extent of its meadows would be a useful approach to estimate the impacts of natural and anthropogenic stressors. Here, we aimed to map the *Z. noltei* meadows in the Merja Zerga coastal lagoon (Atlantic coast of Morocco) using remote sensing. We used a random forest algorithm combined with field data to classify a SPOT 7 satellite image. Despite the difficulties related to the non-synchronization of the satellite images with the high tide coefficient, our results revealed, with an accuracy of 95%, that dwarf eelgrass beds can be discriminated successfully from other habitats in the lagoon. The estimated area was 160.76 ha when considering mixed beds (*Z. noltei*-associated macroalgae). The use of SPOT 7 satellite images seems to be satisfactory for long-term monitoring of *Z. noltei* meadows in the Merja Zerga lagoon and for biomass estimation using an NDVI–biomass quantitative relationship. Nevertheless, using this method of biomass estimation for dwarf eelgrass meadows could be unsuccessful when it comes to areas where the NDVI is saturated due to the stacking of many layers.

Keywords: seagrass; remote sensing; random forest; vegetation indices; machine learning classification

Citation: Benmokhtar, S.; Robin, M.; Maanan, M.; Bazairi, H. Mapping and Quantification of the Dwarf Eelgrass *Zostera noltei* Using a Random Forest Algorithm on a SPOT 7 Satellite Image. *ISPRS Int. J. Geo-Inf.* **2021**, *10*, 313. https://doi.org/10.3390/ijgi10050313

Academic Editor: Wolfgang Kainz

Received: 25 February 2021
Accepted: 2 May 2021
Published: 7 May 2021

1. Introduction

Seagrass meadows exist in most shallow, sheltered, soft-bottomed marine coastlines and estuaries throughout the world and rank among the most productive systems in the ocean [1–3]. They fulfill important trophic and structural functions in the coastal ecosystems [4–6] and rank among the priority habitats classified by the Convention on Biological Diversity (1992). They have been listed as one of the five biological quality elements to be included in ecological quality assessments in marine waters by the European Water Framework Directive (2000/60/EC) [7]. Therefore, due to the widespread decline of seagrass beds on a global scale [1], monitoring these ecosystems is a fundamental step for any program to manage these key habitats. Many techniques are used for monitoring seagrass beds, however the most used indices worldwide relate to their extent, fragmentation, bathymetric limits (colonization of the lower depth), abundance, recovery rate, biomass, density, canopy height and leaf biometry, specific composition and coverage, associated macroalgae, and associated benthic invertebrates [8].

Monitoring of the extent of seagrass meadows is a useful approach to estimate the impacts of natural and anthropogenic stressors. Indeed, this index is the simplest way to study these habitats at both small and large scales [9]; it has a minimal impact on the environment and can prove signs of degradation and suggest the presence of anthropogenic disturbances such as eutrophication, changes in the use of space, and increasing aquatic

activities. In addition, the presence or absence of seagrass beds or their regional distribution defines the limits for the sampling of the cover, biomass, or density along depth gradients, which are supplementary indicators of health of seagrass beds [8].

The dwarf eelgrass *Z. noltei* Hornemann, 1832, is one of the predominant global species in intertidal zones, thus representing the land–sea interface [10]. The distribution of *Z. noltei* extends from the eastern Atlantic shores starting from Mauritania to southern Norway and the Kattegat Sea, and throughout the Mediterranean, Black, Azov, Caspian, and Aral Seas and the Canary Islands [11–13]. *Z. noltei* beds represent a habitat which allows the spatial structuring of many biological communities and are considered the basis of exceptional trophic compartments for many primary consumers [14]. Moreover, *Z. noltei* beds can contribute quantitatively to the function of tidal flats, as they are an extended juvenile habitat for some of the extremely important species in the food web [15]. Indeed, Bououarour et al. [16] showed that macrofaunal biomass has a significant positive relationship with the presence of dwarf eelgrass. They demonstrated that variations in the macrobenthic faunal structure are mainly due to the existence of *Z. noltei*. In semi-enclosed coastal areas, this species is particularly vulnerable to climate-change-derived effects and to anthropogenic pressures [17]. Despite the fact that *Z. noltei* is listed as a species of minor concern by the International Union for the Conservation of Nature (IUCN), the overall population is reported to be declining. *Z. noltei* forms meadows mainly within the intertidal zone, which make it likely to be vulnerable, in particular to climate-change-derived effects, mainly the sea water temperature and increasing sea level rise (SLR), which will affect the state, composition, and evolution of occupied areas, ranging from homogeneous sectors to fragmented patches scattered on the foreshores [14,18–20].

Studies over time have shown that remote sensing applications for seagrass ecosystems represent good tools for monitoring. This can be achieved at a primary level (detection of seagrasses, spatial coverage, species-level discrimination, biomass detection, growth patterns, and degradation) or at a secondary level (environmental variables influencing seagrasses, such as sea surface temperature (SST), salinity, sea level rise, pollution, detection of epiphytes, etc.) [21–25]. The combination of remote sensing techniques with field surveys is essential when monitoring seagrass statuses and changes over long time scales in large regions [26–28]. *Z. noltei* meadows are the most dominant seagrass areas in semi-enclosed coastal systems (SECS) of the Atlantic coast of Morocco [29,30]. Aspects related to mapping and long-term monitoring of dwarf eelgrass are very incomplete or even absent.

The present study aimed to map *Z. noltei* meadows in the Merja Zerga coastal lagoon using a SPOT 7 image provided by the Royal Center for Remote Sensing, along with field data. This is a first step towards future monitoring and an important tool for the management of *Z. noltei* meadows along the Atlantic coast of Morocco.

2. Materials and Methods

2.1. Study Area

The Merja Zerga lagoon, also called Moulay Bousselham lagoon, is a RAMSAR wetland. It is the most northern coastal lagoon along the Atlantic Moroccan coast and is located approximately 120 km north of Rabat, between 34°47′ and 34°53′ north and 6°13′ and 6°19′ west. This lagoon receives daily influence from the Atlantic tides, which are considered the main source of its volume water. It also receives fresh water from two main inflows—the Nador Canal, which is of artificial origin and includes drainage water, as well as the Drader River. Moreover, the lagoon undergoes significant anthropogenic changes [31]. Indeed, the population bordering this lagoon has increased by 150% in the last 25 years [32].

This lagoon's waters are characterized by temperatures ranging from 27 to 28 °C in summer and from 13 to 15 °C in winter [33]. The depth of the lagoon fluctuates between 0 and 2 m but does not exceed 50 cm on average according to the tidal cycle and the precipitation [34,35]. The tide has a mean tidal range of nearly 1.4 m, which increases to 3.60 m during the spring tide, while during the neap tide it decreases to about 0.80 m [36].

The Merja Zerga lagoon provides important socioeconomic support to the local communities through many activities such as tourism and fisheries. Furthermore, it represents a significant ecological resource that has attracted the interest of many scientific researchers. This lagoon has been part of the CASSARINA and MELMARINA projects during the last two decades [37]; thus, several studies have been based on observations and fieldwork in the Merja Zerga, mainly treating hydrological characteristics, environmental changes, contaminants in sediments, plankton, and fish fauna [34,35,38–42].

2.2. Field Data

Seagrass samples were taken from seven dwarf eelgrass stations on 4–5 November 2019, and on 11 November 2019 they were chosen randomly depending on the tidal conditions and scattered on all of the discernible aquatic vegetation areas (pass, east, west and center of the Merja Zerga lagoon) from field investigations and satellite image observations (Table 1, Figure 1).

Table 1. *Z. noltei* field sampling stations in the Merja Zerga lagoon.

Station	S1	S2	S3	S4	S5	S6	S7
Location of the station	Pass 1	Pass 2	Pass 3	Center 1	Center 2	East	West

In order to define the spectral separability of the species lagoon and the mixtures, spectral measurements were performed in situ using a JAZA0478 spectroradiometer with a 348.95–1039.85 nm wavelength range, provided by the LETG laboratory of the University of Nantes. In each station, the reflectance of different types of habitats, in particular the dwarf eelgrass *Z. noltei*, macroalgae (chlorophyte and Rhodophyta), sand, and mud sediments, were recorded at 1 m above ground. For each type of habitat, an average of three to four spectral measurement were sampled in each station and their corresponding references were also taken. The white and dark references were calculated by measuring the reflectance of the white reference (Spectralon® WS-1-SL) and dark reference (performed by covering the collimating lens with its cap).

In order to estimate the *Z. noltei* biomass in g/m^2 and its cover percentage, seven stations were sampled on 16 September 2018 in the intertidal area located in the downstream, upstream, and center of the lagoon during low tide. Biomass was assessed using hand cores (30 cm in length and 12 cm in diameter), with ten replicates for each station. The samples were randomly collected from *Z. noltei* meadows, were washed in situ and taken to the laboratory, then frozen at −20 °C before biomass measurements. The samples before being weighed were oven-dried at 60 °C for two days. As for estimating the cover percentage of the *Z. noltei*, in each station, five replicates of quadrats ($0.5 \times 0.5\ m^2$) were photographed and their geographic coordinates were saved for mapping validation. The quadrats photos were processed by ImageJ software according to Stationary Bed Monitoring Protocols for the Water Directive (WFD) *Zostera marina* (L.)—*Z. noltei* Version 3 [43]. When the use of quadrats was not possible, the cover percentage was estimated visually by assigning it to one of the following classes: 0–25%, 25–50%, 50–75%, 75–90%, 100%.

2.3. Satellite Images

To map the distribution of dwarf eelgrass *Z. noltei* in the Merja Zerga lagoon, we tried to obtain very good images with high resolution, at low tide and with a good tidal coefficient. This was achieved by making a list table with the dates of low tides, coefficients, and the number of images that contained little cloud. Unfortunately, the results were very limited; we must say that this added to the difficulty of achieving very good images. Consequently, we used one SPOT 7 satellite image acquired on 19 August 2019 at 10:54 a.m local time, matching with the falling tide. Indeed, 19 August 2019 corresponds to the lowest tide, which was 0.7 m at 11:46 a.m UTC+1, with a tidal coefficient equal to 72. Images

were obtained during the summer, which is the period of increased density of eelgrass beds, culminating in August–September [44]. In fact, among many Sentinel 2 and Pleiades images, the SPOT 7 image presented the best conditions required for mapping dwarf eelgrass in the Merja Zerga lagoon.

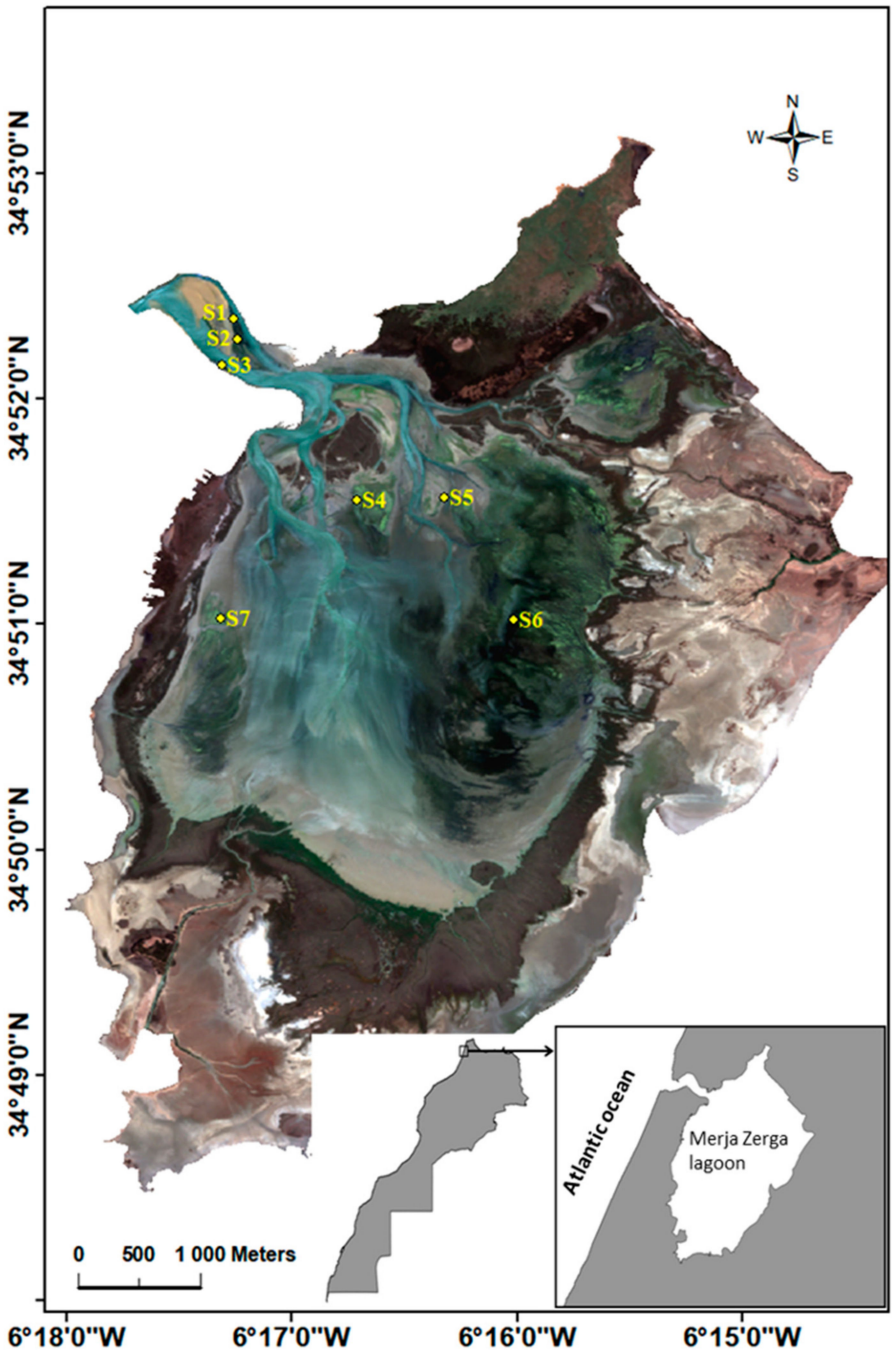

Figure 1. *Z. noltei* sampling stations in the Merja Zerga lagoon: S1, S2, S3, S4, S5, S6, S7 (source: Image SPOT 7).

The SPOT 7 satellite has four multispectral bands—blue (450–520 nm), green (530–590 nm), red (625–695 nm), and near-infrared (NIR; 760–890 nm)—at a spatial resolution of 6 × 6 m, and one panchromatic band (450–745 nm) at a spatial resolution of 1.5 × 1.5 m [45]. The scene was free from cloud cover and was provided by the CRTS (The Royal Center for Remote Sensing—Centre Royal de Télédétection Spatiale (crts.gov.ma,

accessed on 25 February 2021)) in a bundle (PAN + XS) format, which was orthorectified and projected to World Geodetic System 1984 datum, EPSG CODE: 4326.

2.4. Typology

In our approach, we mapped the main habitats that form the Merja Zerga lagoon with reference to the floristic typology outlined by Hammada [46] for this lagoon. This typology showed that there are two gradients that influence the vegetation distribution, namely submersion rhythms and salinity. In fact, the submersion gradient allowed the three types of species to be distinguished, which are:

- Hygrophilous species, which colonize wetlands (wet lawns): *Baldellia ranunculoides* (L.) Parl., *Scirpus lacustris* (L.) Palla., *Typha domigensis* (Pers.) Steud., *Mentha aquatica* (L.), *Nasturtium officinale* (R.Br.);
- Aquatic species, some of which thrive in marine environments (*Z. noltei*, *Nitella* sp. (C. A.) Agardh), while the others colonize calm or stagnant waters and can be floating (*Lemna gibba* (L.)) or fixed (*Myriophyllum* sp. (L.), *Potamogeton pectinatus* (L.) Börner);
- Terrestrial species, which develop in generally humid edge habitats during the rainy period (*Centaurea calcitrapa* (L.), *Euphorbia clementei* Boiss., *Solanum nigrum* (L.)).

We aimed to discern between the aquatic species of the Merja Zerga lagoon marine environment. Hence, the classes that were used for the classification were shallow water, sand, mud, terrestrial plants, algae, mixture of algae and dwarf eelgrass, submerged dwarf eelgrass, and emerged dwarf eelgrass.

2.5. Image Processing

The SPOT 7 image used for this study was delivered in bundle (PAN + XS) format. Atmospheric correction for the four bands was achieved by using the GRASS algorithm in order to convert them to reflectance.

Therefore, the spectral and spatial resolutions were suitable for use with the 9 vegetation indices (Table 1). Indeed, mapping of dwarf eelgrass *Z. noltei* in the Merja Zerga lagoon was achieved by using a supervised classification approach applied with a random forest algorithm (Figure 2), which is a model that constructs and combines a large number of base decision trees.

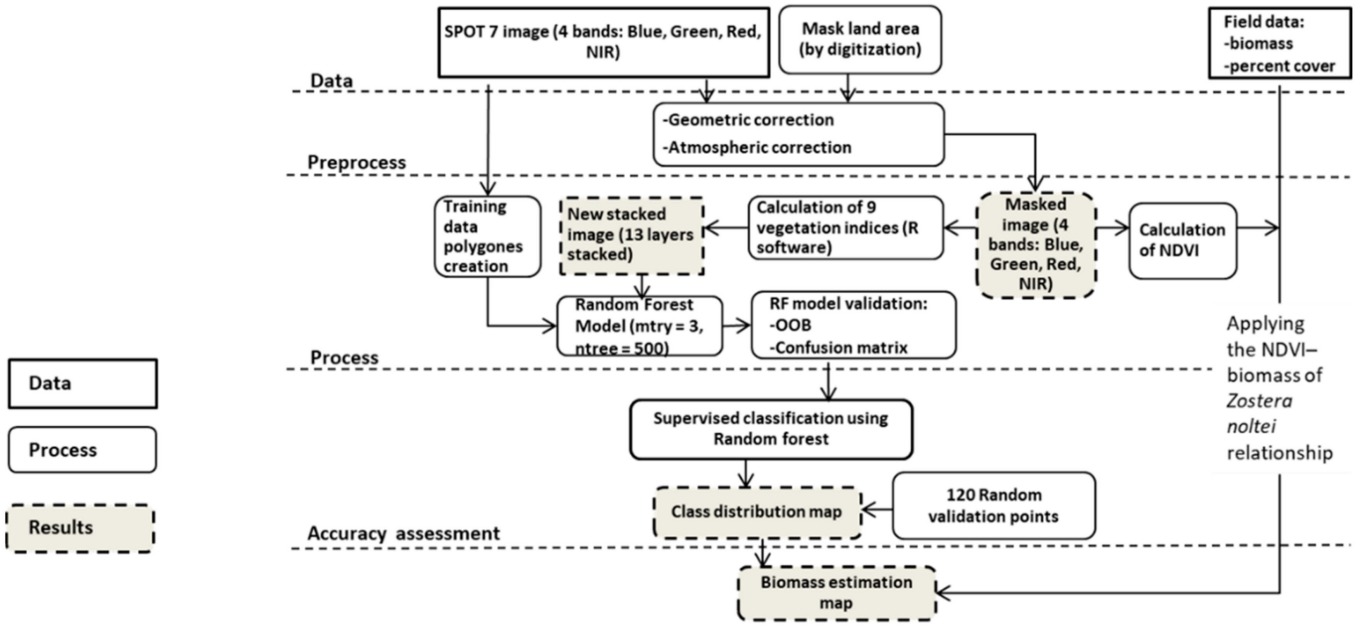

Figure 2. Flowchart of data processing to map dwarf eelgrass *Z. noltei* and algae in the Merja Zerga lagoon.

Before applying the random forest model, 117 polygons were created manually using ArcGIS 10.4.1 software based on personal field knowledge and were distributed over the eight classes, which be used for the classification: shallow water, sand, mud, terrestrial plants, algae, mixture of algae and dwarf eelgrass, submerged dwarf eelgrass, and emerged dwarf eelgrass. For this, we used Breiman and Cutler's random forests for classification and regression algorithm with the R package randomforest v.4.6–14. Known as a robust and consistent model, the random forest algorithm is the most popular ensemble-based model for classification problems, and in particular for seagrass mapping [47]. We empirically tuned the random forests model by testing two parameters (because it seems that there is no theory to guide the choice of the mtry number (number of predictors sampled for spliting at each node) or the number of trees [48]. First, the mtry number was fixed at 3 (with the use of the tuneRF function of the randomForest package). Then, with this mtry number, and in order to find the optimal number of trees that correspond to a stable classifier without excessive computation time, we computed the random forests algorithm with different ntree values and recorded the OOB error rate to assess the number of trees at which the out of bag error rate stabilized and reached the minimum (in our case this was fixed at 500).

First of all, we returned the four raw bands of the SPOT 7 image and used them to calculate nine vegetation indices (Table 2). The resulting layers were then stacked onto a 13-band image, which was then implemented in the random forests model using the R software.

Table 2. SPOT 7 satellite image bands and the 9 indices used for random forests classification.

Bands	Bands and Indices	Band Name and Full Form of Indices
L.1	Band 1	Reflectance in Blue
L.2	Band 2	Reflectance in Green
L.3	Band 3	Reflectance in Red
L.4	Band 4	Reflectance in Near Infra-Red (NIR)
L.5	GNDVI	Green Normalized Vegetation Index [49]
L.6	NDVI	Normalized Vegetation Index [50]
L.7	CVI	Chlorophyll Vegetation Index = (Reflectance in Green–Reflectance in Red)
L.8	GVI	Green Vegetation index [51]
L.9	ICS	Normalized Difference Red/Green, Redness Index [52]
L.10	NLI	Nonlinear Vegetation index [53]
L.11	EVI	Enhanced Vegetation Index [54]
L.12	IB	Brilliance Index [55]
L.13	SAVI	Soil-Adjusted Vegetation Index [56]

The random forests algorithm was validated by the overall out-of-bag (OOB) model error and the confusion matrix (percentage of falsely and classified training pixels) and seemed to be robust (OOB = 3.14). Then, we used the predict function to compute the RF classification prediction with the use of the clusterR interface to speed up the computation (in the R package "raster"). In addition, a final estimation of the quality of the "accuracy" classification error was made using Erdas software by creating 120 equalized random points spread over the eight classes.

To estimate *Z. noltei* aboveground biomass in the Merja Zerga part of the Moulay Bousselham lagoon using remote sensing, we chose to use the quantitative experimental NDVI –*Z. noltei* biomass relationship, whereby biomass = 610.61 (NDVI)^1.88 (n = 31, r2 = 0.97), as created by Barillé et al. (2010). Depending on the presence or absence of algae and the emersion or submersion condition, the precedent equation was separated or combined for the estimated percentage cover (Figure 2).

Hence, a specific biomass estimation map was generated for each of the three classes of *Z. noltei*: two maps were created by directly applying the equation for both the submerged

Z. noltei class and the emerged *Z. noltei* class, and one map was created by combining the equation with the percentage cover of *Z. noltei* for the mixed class of algae and *Z. noltei*.

3. Results

3.1. Spectral Results

According to the spectra, separability between classes was possible. Moreover, the equivalent image calibrated to reflectance also made discrimination between classes possible. The reflectance spectra of algae (n = 9) and *Z. noltei* (n = 13) sampled in the Merja Zerga lagoon presented different overall shapes in the visible and NIR ranges between 400 and 900 nm. Indeed, algae spectra were plotted above the dwarf eelgrass spectra. The distance between algae spectra and emerged dwarf eelgrass spectra was estimated using the spectral angle, which had a value of 0.936 radians. The reflectance spectra of *Z. noltei* were discernible from chlorophyta in the visible wavelengths. However, they had the same tendency (increasing) in the NIR, except for the submerged dwarf eelgrass spectra (decreasing) (Figure 3). The overall shapes of the spectra from the SPOT 7 image we used were similar to those sampled with the spectroradiometer in the field.

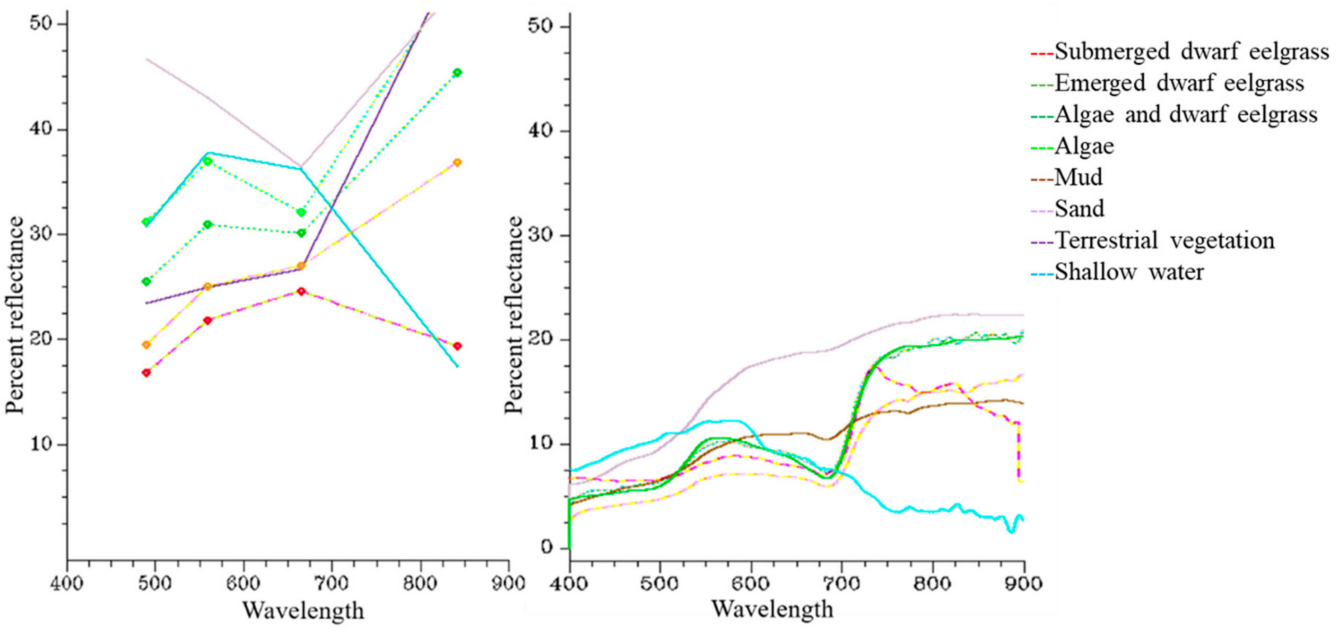

Figure 3. Spectral signatures for the eight different habitat types in the Merja Zerga lagoon: emerged *Z. noltei*, submerged *Z. noltei*, algae, mixed beds of *Z. noltei* and algae, sand, mud, and shallow water. Left: average spectra (n = 5) numbers degraded to the four SPOT 7 satellite image bands: 1 (blue; 450–520 nm), 2 (green; 530–590 nm), 3 (red; 625–695 nm), and 4 (NIR; 760–890 nm). Right: average spectra acquired at the spectral resolution of a JAZA0478 spectroradiometer.

3.2. Biomass and Cover Percentage of *Z. noltei*

Our results showed that the stations S6, S4, and S7 had the highest biomass among the five stations sampled in the Merja Zerga lagoon (Table 3).

Table 3. The average biomass of *Z. noltei* in g/m^2 per station in the Merja Zerga lagoon (stations S3, S4, S5, S6, and S7).

Stations	S5	S3	S4	S7	S6
Average biomass of *Z. noltei* g D.W.m^2	36.17	84.749	96.48	106.448	142.81

According to the visual interpretation and to the quadrat analysis, station S7 had the lowest cover percentage of *Z. noltei*, which was limited to 50% (Table 4).

Table 4. Cover percentage of *Z. noltei* per station in the Merja Zerga (stations S1, S2, S3, S4, S5, S6, and S7; *: insufficient quadrats.

Stations	Cover Percentage of *Z. noltei*		
	September 2017	September 2018	November 2019
S1	0.72	0.92	0.80
S2	0.70	0.72	0.75
S3	0.96	0.94	0.97
S5	0.78	0.76	0.77
S4	– *	0.61	0.60
S7	– *	– *	0.50
S6	– *	– *	0.97

The stations S5 and S4 came in the second position, which were mixed beds (*Z. noltei* and algae) with cover percentages of *Z. noltei* limited to 60% and 75%, respectively. On the contrary, the rest of the stations of the lagoon were homogeneous beds with the highest cover percentages of *Z. noltei*, which reached 96%. In fact, despite their small size, the dwarf eelgrass beds in stations "S3", "S2", and "S1" were homogeneous and denser, plus the presence of macroalgae species there was not very prevalent (Figure 4).

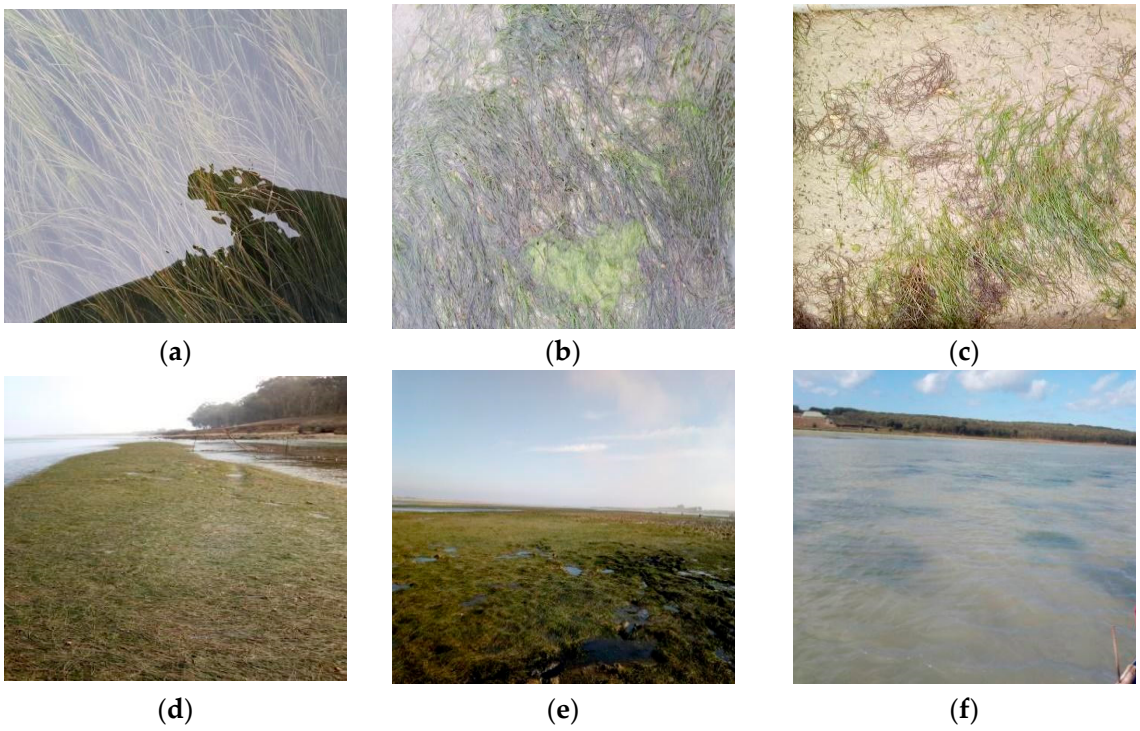

Figure 4. Quadrats of *Z. noltei* in the homogeneous station (**a**) S3 and in mixed stations (**b**) S5 (dense) and (**c**) S7 (sparse, submerged), their respective bed photography (**d**–**f**).

3.3. Satellite Image Processing

Our random forests model accurately predicted the distribution of all eight classes for the Merja Zerga lagoon. The model's internal class errors fluctuated between 0.00 and 0.25% and the OOB for the model was 3.14%. It turned out that the raw bands and indices that were most relevant for distinguishing between the eight classes according to the mean decrease Gini index were the NDVI and GNDVI indices, followed by the GVI, CVI, and EVI, then followed by the green and blue bands successively (Figure 5). Indeed, NDVI and GNDVI indices had the highest mean decrease Gini values, which reached 141.03 and 138.69, respectively.

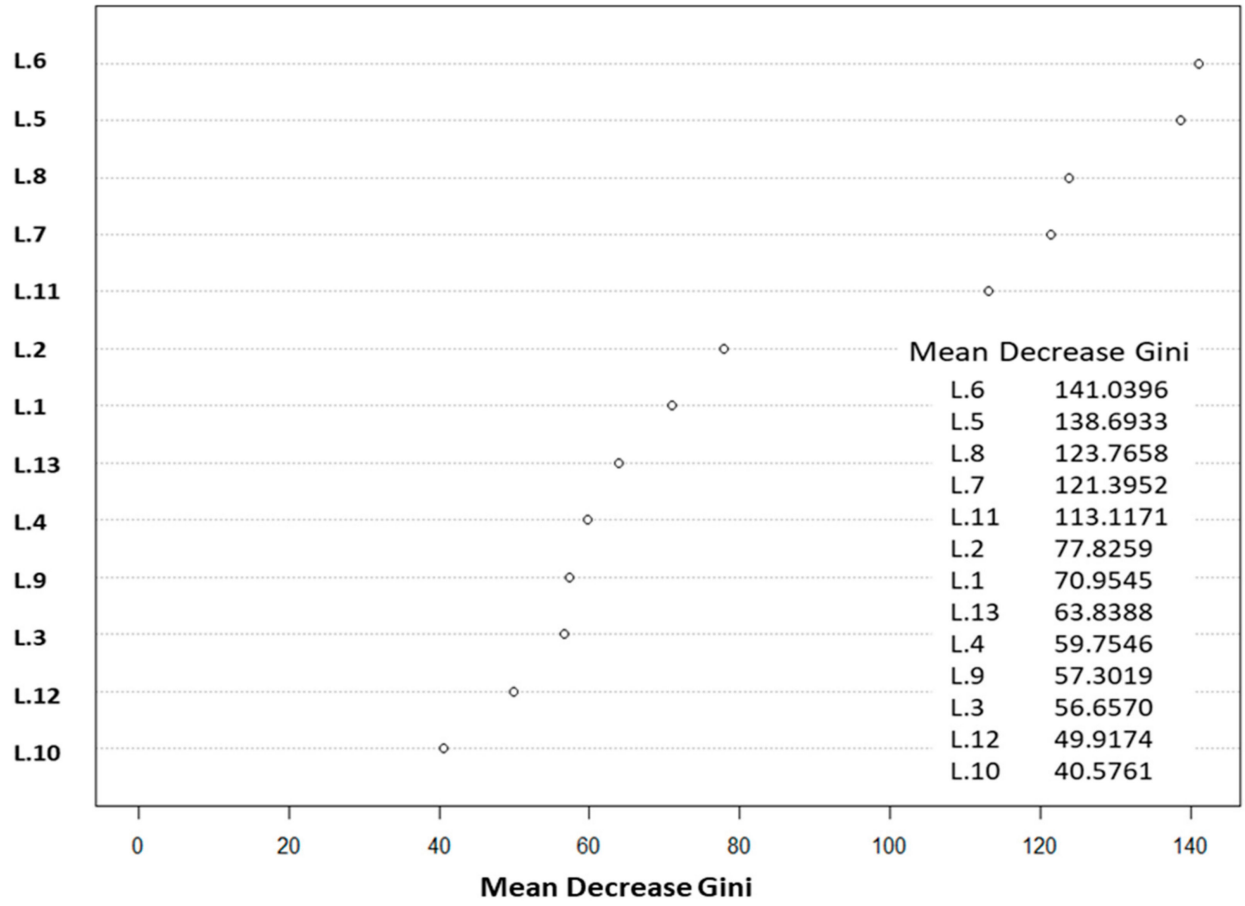

Figure 5. Random forest results: mean decrease Gini values for the 13 bands (L.1: band 1; L.2: band 2; L.3: band 3; L.4: band 4; L.5: GNDVI; L.6: NDVI; L.7: CVI; L.8: GVI; L.9: ICS; L.10: NLI; L.11: EVI; L.12: IB; L.13: SAVI).

The average curve of the pixels per class extracted from the SPOT 7 image showed that each class had a specific band or index which best discriminated it. For example, the IB index was the most relevant for distinguishing submerged dwarf eelgrass (Figure 6).

3.4. Image Classification

We managed to estimate the surface areas of *Z. noltei* meadows in the Merja Zerga lagoon, which was approximately equal to 160.76 ha (mixed beds included), of which 65.22 ha was the total area for emerged and submerged *Z. noltei*.

The classification results indicated that *Z. noltei* beds are more extensive in the center and in the upstream area of the lagoon than in it downstream area (Figure 7), in particular at station S6 (Table 5), which was in agreement with the field observations. Thus, the total surface areas for *Z. noltei* beds were 27.31 ha, 95.54 ha, and 37.91 ha for submerged, mixed, and emerged beds, respectively.

Table 5. The surface areas in ha estimated for *Z. noltei* meadows for each station in the Merja Zerga lagoon: S1, S2, S3, S4, S5, S6, S7.

Classes of *Z. noltei* beds	S6	S7	S5	S4	S3	S1 and S2
Submerged *Z. noltei*	14.08	5.83	1.23	4.58	0.0888	1.49
Emerged *Z. noltei*	31.52	4.67	0.179	1.25	0.0094	0.286
Mixed patches	50.26	24.74	12.26	7.93	0.0736	0.26

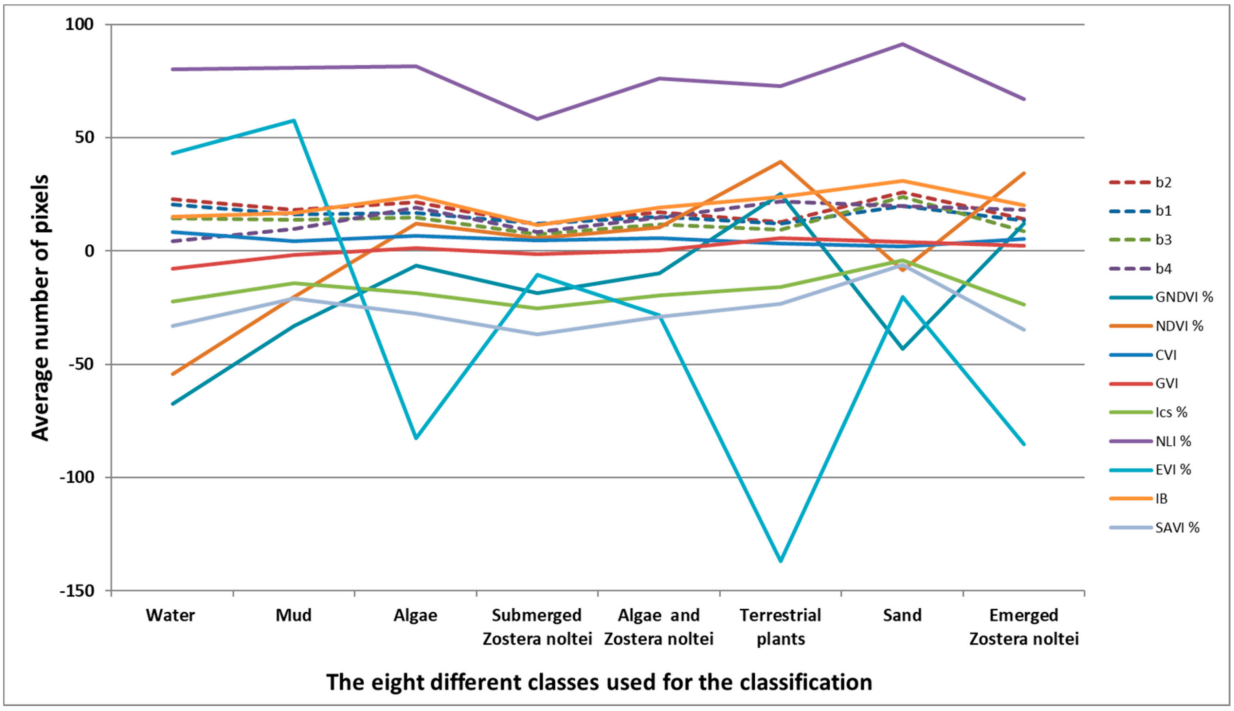

Figure 6. The average of 1371 pixels per class for each of the 4 Bands and 9 indices of the SPOT 7 image.

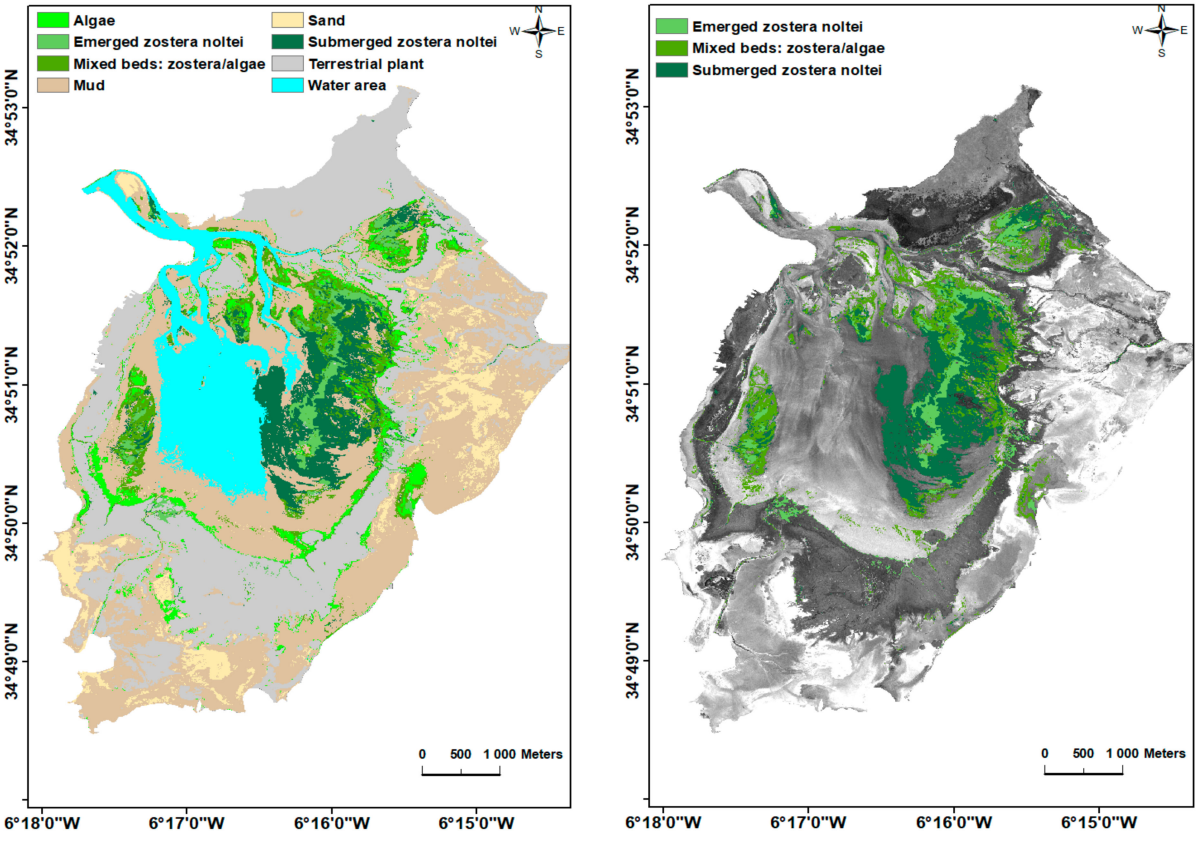

(**a**) (**b**)

Figure 7. (**a**) Random forest classification results and (**b**) the distribution of dwarf eelgrass *Z. noltei* and macroalgae in Moulay Bousselham lagoon.

Dwarf eelgrass biomass results were estimated using remote sensing ranges between 0 and 277.81 g DW/m^2 for the class "emerged *Z. noltei*" and between 0 and 156.509 g DW/m^2 for the class "mixed beds", of which 62% (which is the average of the three mixed station: "S5":0.77, "S4":0.60, "S7":0.50) corresponded to *Z. noltei*, i.e., was between 0 and 97.03 g DW/m^2. Lastly, biomass values were between 0 and 160.79 g DW/m^2 for the class "submerged *Z. noltei*" (Figure 8).

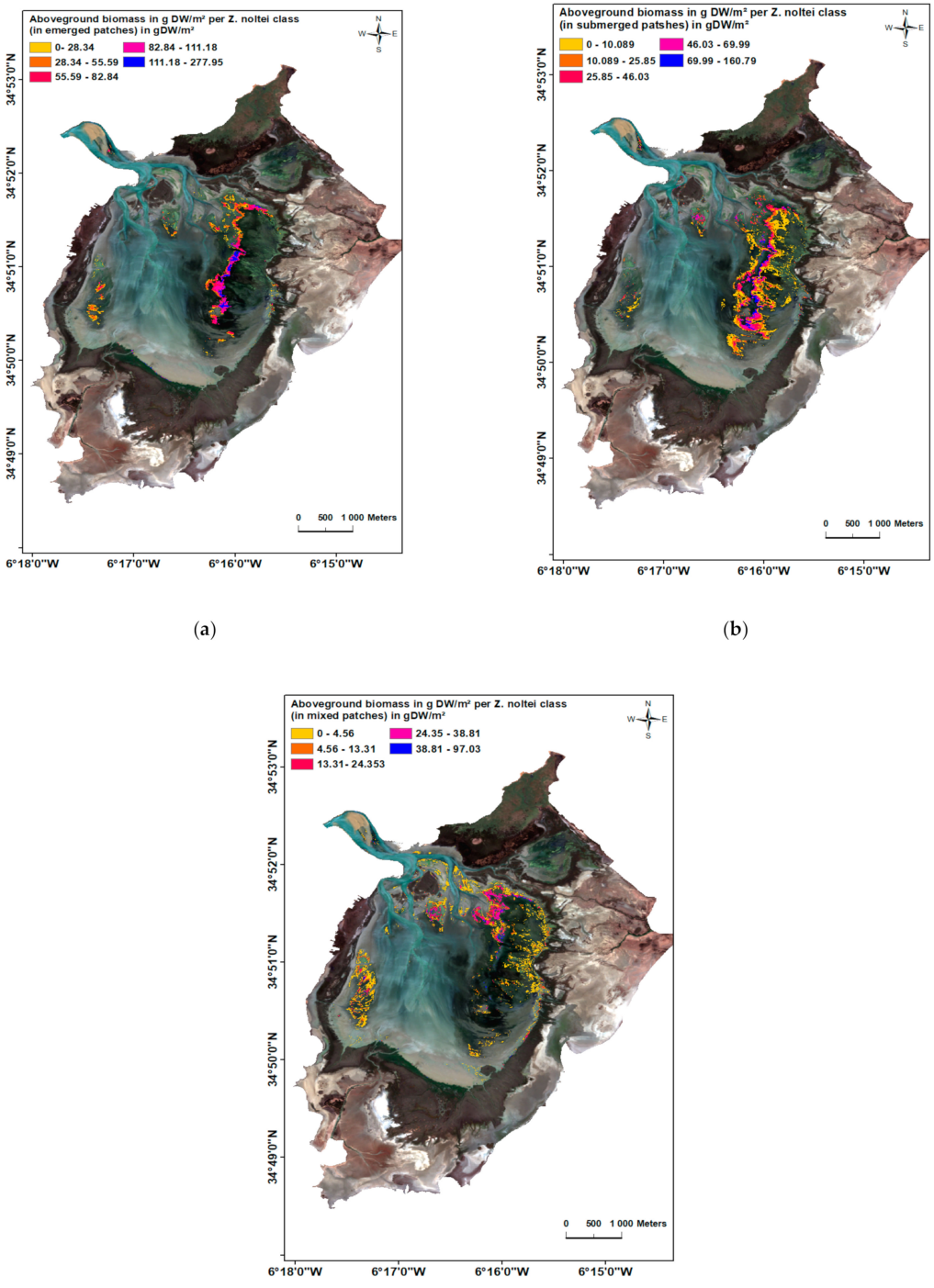

Figure 8. Aboveground biomass in g DW/m^2 per *Z. noltei* class (**a**–**c**) in the Merja Zerga lagoon.

4. Discussion

The overall shapes of the spectral signature of the algae and the dwarf eelgrass found in the field look like those obtained by Bargain et al. [54] and by Dehouck et al. [57]. In fact, *Z. noltei* reflectance is discernible from green algae in the visible wavelengths and even more in the NIR wavelength. In addition, emerged dwarf eelgrass and algae spectra increase in the NIR wavelength compared to the submerged dwarf eelgrass spectra, which have a decreasing slope due to the residual water layers in them. This is due to the influence of water. Dehouck et al. [57] indicated that in general the spectra of *Z. noltei* and algae are similar, however small differences are noticeable in narrow bands. They claimed that the spectra need to be analyzed and separated numerically to find out the best spectral bands.

We chose to use vegetation indices to map *Z. noltei* in the Merja Zerga lagoon because it exists in the form of monospecific seagrass beds. Indeed, the average curve for pixels per class extracted from the SPOT 7 image showed that each class has a specific band or index which best discriminated it. For example, the IB index is the most relevant for distinguishing submerged dwarf eelgrass (Figure 6). Our OOB and mean decrease Gini results showed that NDVI, GNDVI, GVI, and CVI are the best indices to use for this purpose (Figure 5). The mapping of seagrass meadows using multispectral and hyperspectral images has often been achieving by using the NDVI, which is the most widely used index to assess green biomass [58]. Indeed, Barillé et al. [59] calibrated SPOT 7 images to NDVI and tested the influence of *Z. noltei* aboveground biomass variations on spectral reflectance. Hence, they used field-measured hyperspectral data from seagrass and algae and then applied a quantitative experimental NDVI–biomass relationship to map the biomass distribution of *Z. noltei*. The latter displayed a characteristic steep slope from 700 to 900 nm, which increased with increasing biomass. Later, Bargain et al. [60] demonstrated that vegetation indices used to map these kinds of beds and their biomass with satellite or airborne imagery must be selected carefully to moderate all sources of variability affecting the index value, such as the pigment variations, or those related to background influences, such as the soil spectral contrast, albedo variations, or the specular reflectance at the leaf surfaces.

Our study is the first study of the mapping of *Z. noltei* beds using a random forest algorithm. This method showed satisfying results because it has been proven effective to estimate the surface distributions of this species using SPOT 7 satellite imagery. Our mapping results showed that *Z. noltei* beds in the Merja Zerga lagoon are more extensive than in the older studies [61,62]. Indeed, their surface area reached 65.22 ha, and when including associated seaweed mats, this equaled 160.76 ha (Table 6).

Table 6. Surface area for *Z. noltei* at each station in the Merja Zerga lagoon: S1, S2, S3, S4, S5, S6, S7.

***Z. noltei* Beds Surfaces (ha)**	**S6**	**S7**	**S5**	**S4**	**S3**	**S1 and S2**
Total surface area of *Z. noltei* and algae (ha)	95.86	35.24	13.68	13.76	0.17	2.05
Cover percentage of *Z. noltei*	0.97	0.5	0.77	0.61	0.96	0.77
Z. noltei surface area (ha)	92.98	17.61	10.53	8.39	0.16	1.57

Usually, mapping *Z. noltei* meadows by using a handheld GPS instrument or by using transects is not enough when some areas are inaccessible due to the nature of the substrate, to the extent of the meadows, and to the tidal cycles. Generally, estimating seagrass distributions using traditional methods with pre-recorded grid patterns or a combination of transects and sampling points [63] is time-consuming and has high associated costs [10]. This can, therefore, be achieved thanks to remote sensing, either by interpretating aerial photographs from an unmanned aerial vehicle (UAV) combined with ground truthing measurements [4–7] or by terrestrial, oblique, large-scale photography and satellite image classification [64–67].

Some studies also proved the efficiency of random forest approaches in mapping the extent of seagrass. Indeed, according to Traganos and Reinartz [68], the random forest

machine learning classifiers and support vector machines are gaining more interest for coastal habitat remote sensing. Indeed, they assessed the extent of change for *Posidonia oceanica* (L.) Delile and *Cymodocea nodosa* (Ucria) Ascherson following atmospheric and analytical water column correction and using a random forest algorithm for the RapidEye time series. Furthermore, Zhang [69] and Traganos and Reinartz [70] proved that random forest algorithms generated promising results regarding classification of seagrasses, while Zhang et al. [71] exhibited the advantages of al. [57] emphasizes that by carefully selecting multispectral bands or by combining them random forest algorithms over the maximum likelihood classifier using hyperspectral imagery.

In contrast to our study, several previous studies have mentioned the presence of *Z. noltei* in Merja Zerga lagoon, but without giving its overall distribution. First, Dakki et al. [61] estimated that 4.78% of the lagoon's surface was occupied by dwarf eelgrass meadows, the surface area of which corresponded to 140 ha, including algae species. The presence of *Z. noltei* in the Merja Zerga lagoon was also reported by Boutahar et al. [30], Gam et al. [72], Grignon-Dubois and Rezzonico [73], Natij et al. [74], Touhami et al. [75], and Touhami et al. [76]. The dwarf eelgrass meadows in this lagoon have developed in muddy and sometimes deep substrates, which makes walking through them very difficult, so mapping these meadows on foot is not feasible. Lately, according to Zarranz Elso et al. [62], dwarf eelgrass has been mapped in the Merja Zerga lagoon through spectral characterization and a maximum likelihood classification of a World View 2 satellite image acquired on 3 November 2010, combined with field samples. Hence, the surface area of *Z. noltei* meadows in Merja Zerga lagoon was estimated to be 71.508 m^2, however in this case the satellite image used did not cover all of the intertidal areas of the lagoon. However, this study missed the bigger beds located in the downstream area of the lagoon. When interpreting multispectral optical images, confusion persisted between dwarf eelgrass meadows, algae, and the cordgrass *Spartina* sp., which is an emergent halophilous species that boarders the lagoon with other saltmarsh species, especially *Salicornia sp.* (L.) and Juncaceae rushes [62,75]. Dehouck et using a multitemporal database they could limit this confusion, and that algae seem to be discriminable only when using fine spectral bands. According to Proença et al. [77], the mapping of *Spartina anglica* C.E. Hubb. and *Spartina maritima* (Curtis) Fernald using supervised classification of Pleiades images showed that these species were often confused with the vast areas vegetated by *Z. noltei*, in particular in October. In order to achieve better results and to avoid this confusion, it is better to mask the majority of the potential terrestrial vegetation from the satellite image before running the classification algorithm. In our case, this problem did not occur because we created a sufficient number of polygons (117) distributed across the eight classes used for the classification. In fact, based on the accuracy assessment results, the random forest classification generated a satisfactory *Z. noltei* meadow map, with a kappa index equal to 0.9429 and an overall accuracy equal to 95%.

Our classification results allowed the estimation of the overall extent of *Z. noltei* in the Merja Zerga lagoon and also allowed the estimation of the aboveground biomass of this species. As with the study by Barillé et al. [60], in our case the NDVI–biomass quantitative relationship was applied to all *Z. noltei* meadows successfully, because despite the stacking of many layers in certain areas, the NDVI was not saturated. Thus, this method was applied directly for the classes "emerged *Z. noltei*" and "submerged *Z. noltei* " and was combined with the cover percentage for the class "mixed *Z. noltei* and algae". Indeed, we observed during field investigations that *Z. noltei* was not the main living macrophyte in the mapped intertidal area—filamentous green macroalgae was observed in the mixed beds and a few macroalgae species (Cholorophyta and Rhodophyta) were occasionally present (Figure 9).

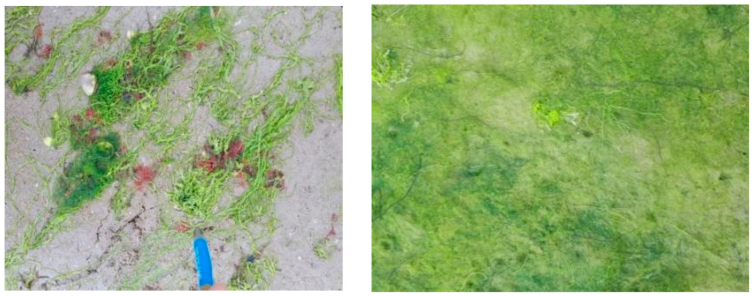

(**a**) (**b**)

Figure 9. Macroalgae species associated with *Z. noltei* (**a**) and filamentous green macroalgae (**b**) in the mixed beds observed in the intertidal area of the Merja Zerga lagoon.

Indeed, Valle et al. [78] claimed that the NDVI is useful for distinguishing between sparsely vegetated and dense *Z. noltei* beds, and therefore can be further applied to CASI (hyperspectral sensor) imagery to map the cover percentages of the species living in the area.

The calibration of the SPOT 7 image with the biomass–NDVI relationship showed a pattern of maximal biomass in the submerged and emerged classes, especially in the "S6" station, and lower biomass in the center zone ("S5" and "S4" stations). The average biomass measured in situ in September 2018 was not significantly different from the value obtained from remote sensing (Table 7).

Table 7. The average biomass for *Z. noltei* in g/m^2 for each station in the Merja Zerga lagoon: S1, S2, S3, S4, S5, S6, S7.

***Z. noltei* Classes**	**Mixed Beds**		**Submerged/Emerged Beds**		
Maximum biomass of *Z. noltei* g D.W.m^2 (from SPOT 7 image calibration)	97.03		160.79/277.95		
Stations	**S5**	**S4**	**S3**	**S6**	**S7**
Average biomass of *Z. noltei* g D.W.m^2 (from field samples)	36.17	96.48	77.62 to 84.749	142.81	106.448

Lately, active remote sensing data from aircrafts or UAVs have been used to map seagrass cover, mainly LiDAR [78–86]; hyperspectral sensors such as CASI-2, PHILLS, and HyMap [78,87–90]; or photographs [91–95]. The efficiency of remotely sensed data has been proven through many studies involving the estimation of seagrass cover; nevertheless, most studies are still reliant on field measurements when estimating shoot density and canopy height (e.g., [96]).

5. Conclusions

In our study, the suitability of using remote sensing to firstly map the distribution of *Z. noltei* and secondly to estimate its biomass was confirmed. In fact, we classified a SPOT 7 satellite image using a random forest algorithm and field data to produce dwarf eelgrass habitat maps. This approach enabled us to define the distribution of *Z. noltei* beds and associated macroalgae in terms of surface coverage. Our results proved with an accuracy of 95% that GNDVI, NDVI, and EVI are potentially useful vegetation indices for discriminating dwarf eelgrass beds from other habitats in the lagoon. Older maps involving the spatial characterization of *Z. noltei* in the Merja Zerga lagoon could not determine the entire extent of this seagrass. Compared to our work, previous studies on *Z. noltei* mapping underestimated its extent due to the fact that they used images that did not fit all of the Merja Zerga lagoon or were taken at a higher tide. Indeed, the overall surface occupied by dwarf eelgrass in this wetland is 160.76 ha when considering mixed beds. Our approach

was based on estimating the extent, which is a global index that can reveal the increase or loss of the area of seagrass beds at its limits; it does not consider the losses inside these limits, which are visible at the level of the fragmentation of these beds. Biomass estimation of dwarf eelgrass using the NDVI–biomass quantitative model applied to SPOT 7 images can be very useful as a non-destructive method for estimating the biomass of this seagrass species. In future studies of *Z. noltei* and in order to purchase the data obtained, the same methodology should be considered.

Author Contributions: Conceptualization, Salma Benmokhtar, Marc Robin, and Hocein Bazairi; metholodogy, Salma Benmokhtar, Marc Robin, and Hocein Bazairi; field data acquisition, Salma Benmokhtar, Marc Robin, Hocein Bazairi, and Mohamed Maanan; writing—review and editing, Salma Benmokhtar, Marc Robin, Hocein Bazairi, and Mohamed Maanan. All authors have read and agreed to the published version of the manuscript.

Funding: This research received no external funding.

Institutional Review Board Statement: Not applicable.

Informed Consent Statement: Not applicable.

Data Availability Statement: Not applicable.

Acknowledgments: The authors thank Ouassal Keltoum, Louizi Halima, Tifarouine Loubna, Boutahar Loubna, Boutoumit Soilam for providing their help during field data acquisition; El Mahsani Abderahman and Maanan Mehdi for their help in my initiation to GIS and remote sensing.

Conflicts of Interest: The authors declare no conflict of interest.

References

1. Orth, R.J.; Carruthers, T.J.; Dennison, W.C.; Duarte, C.M.; Fourqurean, J.W.; Heck, K.L.; Hughes, A.R.; Kendrick, G.A.; Kenworthy, W.J.; Olyarnik, S. A Global Crisis for Seagrass Ecosystems. *Bioscience* **2006**, *56*, 987–996. [CrossRef]
2. Duarte, C.; Borum, J.; Short, F.T.; Walker, D.I. Seagrass Ecosystems: Their Global Status and Prospects. In *Aquatic Ecosystems: Trends and Global Prospects*; Cambridge University Press: Cambridge, UK, 2008; pp. 281–294. [CrossRef]
3. Short, F.T.; Polidoro, B.; Livingstone, S.R.; Carpenter, K.E.; Bandeira, S.; Bujang, J.S.; Calumpong, H.P.; Carruthers, T.J.B.; Coles, R.G.; Dennison, W.C.; et al. Extinction risk assessment of the world's seagrass species. *Biol. Conserv.* **2011**, *144*, 1961–1971. [CrossRef]
4. Duffy, J. Biodiversity and the functioning of seagrass ecosystems. *Mar. Ecol. Prog. Ser.* **2006**, *311*, 233–250. [CrossRef]
5. Short, F.; Carruthers, T.; Dennison, W.; Waycott, M. Global seagrass distribution and diversity: A bioregional model. *J. Exp. Mar. Biol. Ecol.* **2007**, *350*, 3–20. [CrossRef]
6. Gutiérrez, J.L.; Jones, C.G.; Byers, J.E.; Arkema, K.; Berkenbusch, K.; Commito, J.A.; Duarte, C.M.; Hacker, S.D.; Lambrinos, J.G.; Hendriks, I.E.; et al. Physical Ecosystem Engineers and the Functioning of Estuaries and Coasts. In *Treatise on Estuarine and Coastal Science*; Academic Press: Waltham, MA, USA, 2011; Volume 7, pp. 53–81.
7. Marbà, N.; Krause-Jensen, D.; Alcoverro, T.; Birk, S.; Pedersen, A.; Neto, J.M.; Orfanidis, S.; Garmendia, J.M.; Muxika, I.; Borja, A.; et al. Diversity of European seagrass indicators: Patterns within and across regions. *Hydrobiologia* **2012**, *704*, 265–278. [CrossRef]
8. Fontan, E.; Dumas, P.; Ponton, D. Méthodes de Cartographie, de Caractérisation et de Suivi des Herbiers Marins. 2011. Available online: https://www.google.com/url?sa=t&rct=j&q=&esrc=s&source=web&cd=&cad=rja&uact=8&ved=2ahUKEwjenJLGiLHwAhWJFMAKHcgtA4gQFjAAegQIAxAD&url=https%3A%2F%2Fwww.zoneco.nc%2Fsystem%2Ffiles_force%2Fdocuments%2Fmethode_de_cartographie_de_caracterisation_et_de_suivi_des_herbiers_marins.pdf%3Fdownload%3D1&usg=AOvVaw3mGzT8NjBkgJVlHJK_Yj1R (accessed on 25 February 2021).
9. Borum, J.; Duarte, C.M.; Krause-Jensen, D.; Greve, T.M. *European Seagrasses: An Introduction to Monitoring and Management*; The EU Project Monitoring and Management of European Seagrasses (M&MS Project): Hilleroed, Danmark, 2004; ISBN 87-89143-21-3.
10. Short, F.T.; Coles, R.G. *Global Seagrass Research Method*; Elsevier Science B.V.: Amsterdam, The Netherlands, 2001; 473p.
11. Green, E.R.; Short, F.T. *World Atlas of Seagrasses*; University of California Press: Berkeley, CA, USA, 2003.
12. Moore, K.A.; Short, F.T. Zostera: Biology, ecology and management. In *Seagrasses: Biology, Ecology and Conservation*; Larkum, T., Orth, R., Duarte, C., Eds.; Springer: Dordrecht, The Netherlands, 2006; pp. 361–386.
13. Diekmann, O.E.; Gouveia, L.; Perez, J.A.; Gil-Rodriguez, C.; Serrão, E.A. The possible origin of Zostera noltii in the Canary Islands and guidelines for restoration. *Mar. Biol.* **2010**, *157*, 2109–2115. [CrossRef]
14. Dalloyau, S. Qualité Ecologique des Herbiers Intertidaux à Zostère Naine Zostera Noltei dans les Sites Fonctionnels des Réserves Naturelles Nationales Gérées par la LPO (Pertuis Charentais). 2020. Available online: https://www.researchgate.net/publication/349345847_Qualite_ecologique_des_herbiers_intertidaux_a_Zostere_naine_Zostera_noltei_dans_les_sites_fonctionnels_des_Reserves_Naturelles_Nationales_gerees_par_la_LPO_Pertuis_Charentais (accessed on 25 February 2021).

15. Polte, P.; Schanz, A.; Asmus, H. The contribution of seagrass beds (*Zostera noltii*) to the function of tidal flats as a juvenile habitat for dominant, mobile epibenthos in the Wadden Sea. *Mar. Biol.* **2005**, *147*, 813–822. [CrossRef]
16. Bououarour, O.; El Kamcha, R.; Boutoumit, S.; Pouzet, P.; Maanan, M.; Bazairi, H. Effects of the Zostera noltei meadows on benthic macrofauna in North Atlantic coastal ecosystems of Morocco: Spatial and seasonal patterns. *Biologia* **2021**, 1–13. [CrossRef]
17. Cabaço, S.; Santos, R.; Sprung, M. Population dynamics and production of the seagrass Zostera noltii in colonizing versus established meadows. *Mar. Ecol.* **2011**, *33*, 280–289. [CrossRef]
18. Chust, G.; Borja, Á.; Caballero, A.; Irigoien, X.; Sáenz, J.; Moncho, R.; Marcos, M.; Liria, P.; Hidalgo, J.; Valle, M.; et al. Climate change impacts on coastal and pelagic environments in the southeastern Bay of Biscay. *Clim. Res.* **2011**, *48*, 307–332. [CrossRef]
19. Massa, S.I.; Arnaud-Haond, S.; Pearson, G.A.; Serrão, E.A. Temperature tolerance and survival of intertidal populations of the seagrass Zostera noltii (Hornemann) in Southern Europe (Ria Formosa, Portugal). *Hydrobiol.* **2008**, *619*, 195–201. [CrossRef]
20. Short, F.T.; Neckles, H.A. The effects of global climate change on seagrasses. *Aquat. Bot.* **1999**, *63*, 169–196. [CrossRef]
21. Chauvaud, S.; Bouchon, C.; Maniere, R. Remote sensing techniques adapted to high resolution mapping of tropical coastal marine ecosystems (coral reefs, seagrass beds and mangrove). *Int. J. Remote Sens.* **1998**, *19*, 3625–3639. [CrossRef]
22. Dekker, A.; Brando, V.; Antsee, J.; Fyfe, S.; Malthus, T.; Karpouzli, A. Remote Sensing of Seagrass Ecosystems: Use of Space-borne and Airborne Sensors. In *Seagrasses: Biology, Ecology and Conservation*; Larkum, T., Orth, R.J., Duarte, C.M., Eds.; Springer: Dordrecht, The Netherlands, 2006; pp. 347–359, ISBN 978-1-4020-2983-7.
23. Ferwerda, J.G.; De Leeuw, J.; Atzberger, C.; Vekerdy, Z. Satellite-based monitoring of tropical seagrass vegetation: Current techniques and future developments. *Hydrobiologia* **2007**, *591*, 59–71. [CrossRef]
24. Hossain, M.S.; Bujang, J.S.; Zakaria, M.H.; Hashim, M. Application of Landsat images to seagrass areal cover change analysis for Lawas, Terengganu and Kelantan of Malaysia. *Cont. Shelf Res.* **2015**, *110*, 124–148. [CrossRef]
25. Hossain, M.S.; Hashim, M. Potential of Earth Observation (EO) technologies for seagrass ecosystem service assessments. *Int. J. Appl. Earth Obs. Geoinf.* **2019**, *77*, 15–29. [CrossRef]
26. Dingtian, Y.; Chaoyu, Y.D.A.Y. Seagrass Distribution in China with Satellite Remote Sensing. In *Remote Sensing of Planet Earth*; IntechOpen: London, UK, 2012; p. 29043. Available online: https://www.intechopen.com/books/remote-sensing-of-planet-earth/seagrass-distribution-in-china-with-remote-sensin (accessed on 25 February 2021).
27. Meyer, C.A.; Pu, R. Seagrass resource assessment using remote sensing methods in St. Joseph Sound and Clearwater Harbor, Florida, USA. *Environ. Monit. Assess.* **2011**, *184*, 1131–1143. [CrossRef]
28. Roelfsema, C.M.; Phinn, S.R.; Udy, N.S.; Maxwell, P.S. An integrated field and remote sensing approach for mapping Seagrass Cover, Moreton Bay, Australia. *J. Spat. Sci.* **2009**, *54*, 45–62. [CrossRef]
29. Bououarour, O.; El Kamcha, R.; Boutahar, L.; Tnoumi, A.; Zourarah, B.; Benhoussa, A.; Bazairi, H. Spatial patterns of the Zostera noltei meadows across the Atlantic coast of Morocco: Is there a latitudinal gradient? *PeerJ PrePr.* **2015**, *3*, e1076v1. [CrossRef]
30. Boutahar, L.; Maanan, M.; Bououarour, O.; Richir, J.; Pouzet, P.; Gobert, S.; Maanan, M.; Zourarah, B.; Benhoussa, A.; Bazairi, H. Biomonitoring environmental status in semi-enclosed coastal ecosystems using Zostera noltei meadows. *Ecol. Indic.* **2019**, *104*, 776–793. [CrossRef]
31. Ahmed, M.H.; El Leithy, B.M.; Thompson, J.R.; Flower, R.J.; Ramdani, M.; Ayache, F.; Hassan, S.M. Application of remote sensing to site characterisation and environmental change analysis of North African coastal lagoons. *Hydrobiologia* **2009**, *622*, 147–171. [CrossRef]
32. Maanan, M.; Landesman, C.; Maanan, M.; Zourarah, B.; Fattal, P.; Sahabi, M. Evaluation of the anthropogenic influx of metal and metalloid contaminants into the Moulay Bousselham lagoon, Morocco, using chemometric methods coupled to geographical information systems. *Environ. Sci. Pollut. Res.* **2013**, *20*, 4729–4741. [CrossRef] [PubMed]
33. Bazaïri, H.; Bayed, A.; Glémarec, M.; Hily, C. Spatial organisation of macrozoobenthic communities in response to envi-ronmental factors in a coastal lagoon of the NW African coast (Merja Zerga, Morocco). *Oceanol. Acta* **2003**, *26*, 457–471. [CrossRef]
34. Kraiem, M.; Ben Hamza, C.; Ramdani, M.; Fathi, A.; Abdelzaher, H.; Flower, R. Some observations on the age and growth of thin-lipped grey mullet, Liza ramada Risso, 1826 (Pisces, Mugilidae) in three North African wetland lakes: Merja Zerga (Morocco), Garâat Ichkeul (Tunisia) and Edku Lake (Egypt). *Aquat. Ecol.* **2001**, *35*, 335–345. [CrossRef]
35. Labbardi, H.; Ettahiri, O.; Lazar, S.; Massik, Z.; El Antri, S. Étude de la variation spatio-temporelle des paramètres physico-chimiques caractérisant la qualité des eaux d'une lagune côtière et ses zonations écologiques: Cas de Moulay Bousselham, Maroc. *CR GEOSCI* **2005**, *337*, 505–514. [CrossRef]
36. Alaoui, A.M.; Choura, M.; Maanan, M.; Zourarah, B.; Robin, M.; Conceição, M.F.; Andrade, C.; Khalid, M.; Carruesco, C. Metal fluxes to the sediments of the Moulay Bousselham lagoon, Morocco. *Environ. Earth Sci.* **2009**, *61*, 275–286. [CrossRef]
37. Flower, R.J.; Thompson, J.R. An overview of integrated hydro-ecological studies in the MELMARINA Project: Monitoring and modelling coastal lagoons—making management tools for aquatic resources in North Africa. *Hydrobiologia* **2008**, *622*, 3–14. [CrossRef]
38. Appleby, P.G.; Birks, H.H.; Flower, R.J.; Rose, N.; Peglar, S.M.; Ramdani, M.; Kraïem, M.M.; Fathi, A.A. Radiometrically determined dates and sedimentation rates for recent sediments in nine North African wetland lakes (the CASSARINA Pro-ject). *Aquat. Ecol.* **2001**, *35*, 347–367. [CrossRef]
39. Peters, A.; Jones, K.C.; Flower, R.; Appleby, P.; Ramdani, M.; Kraiem, M.; Fathi, A. Recent environmental change in North African wetland lakes: A baseline study of organochlorine contaminant residues in sediments from nine sites in the CASSARINA Project. *Aquat. Ecol.* **2001**, *35*, 449–459. [CrossRef]

40. Ramdani, M.; Flower, R.J.; Elkhiati, N.; Kraïem, M.M.; Fathi, A.A.; Birks, H.H.; Patrick, S.T. North African wetland lakes: Characterization of nine sites included in the CASSARINA Project. *Aquat. Ecol.* **2001**, *35*, 281–302. [CrossRef]
41. Ramdani, M.; Elkhiati, N.; Flower, R.J.; Thompson, J.R.; Chouba, L.; Kraiem, M.M.; Ayache, F.; Ahmed, M.H. Environmental influences on the qualitative and quantitative composition of phytoplankton and zooplankton in North African coastal la-goons. *Hydrobiologia* **2009**, *622*, 113–131. [CrossRef]
42. Thompson, J.R.; Flower, R.J.; Ramdani, M.; Ayache, F.; Ahmed, M.H.; Rasmussen, E.K.; Petersen, O.S. Hydrological charac-teristics of three North African coastal lagoons: Insights from the MELMARINA project. *Hydrobiologia* **2009**, *622*, 45–84. [CrossRef]
43. Hily, C.; Sauriau, P.G.; Auby, I. *Protocoles Suivi Stationnel des Herbiers à Zostères pour la Directive Cadre sur l'Eau (DCE) Zostera marina*; Rapport Ifremer/ODDE/UL/LER/AR/18.017; Ifremer: Brest, France, 2007.
44. Wong, M.C.; Bravo, M.A.; Dowd, M. Ecological dynamics of Zostera marina (eelgrass) in three adjacent bays in Atlantic Canada. *Bot. Mar.* **2013**, *56*, 413–424. [CrossRef]
45. Astrium Services. SPOT 6 & SPOT 7 Imagery User Guide. *France.* 2013. Available online: https://www.google.com/url?sa=t&rct=j&q=&esrc=s&source=web&cd=&ved=2ahUKEwj-r6nx_LDwAhWC7eAKHQ8lBF8QFjABegQIAhAD&url=https%3A%2F%2Fwww.spaceoffice.nl%2Fblobs%2FDataportaal%2FUser_Guide_SPOT6_V1.0.pdf&usg=AOvVaw1ppInVLdBsoFQgGFiigs5a (accessed on 25 February 2021).
46. Hammada, S. *Etudes sur la Végétation des zones Humides du Maroc: Catalogue et Analyse de la Biodiversité Floristique et Identification des Principaux Groupements Végétaux, 2017*; Université Mohammed V-Agdal, Faculté des Sciences Rabat: Rabat, Morocco, 27 February 2007.
47. Ha, N.T.; Manley-Harris, M.; Pham, T.D.; Hawes, I. A Comparative Assessment of Ensemble-Based Machine Learning and Maximum Likelihood Methods for Mapping Seagrass Using Sentinel-2 Imagery in Tauranga Harbor, New Zealand. *Remote Sens.* **2020**, *12*, 355. [CrossRef]
48. Scornet, E. Tuning parameters in random forests. *ESAIM: Proc. Surv.* **2017**, *60*, 144–162. [CrossRef]
49. Gitelson, A.A.; Kaufman, Y.J.; Merzlyak, M.N. Use of a green channel in remote sensing of global vegetation from EOS-MODIS. *Remote Sens. Environ.* **1996**, *58*, 289–298. [CrossRef]
50. Rouse, J.W.J.; Haas, R.H.; Schell, J.A.; Deering, D.W. Monitoring vegetation systems in the Great Plains with ERTS. *NASA Spec. Publ.* **1974**, *351*, 309–317.
51. Kauth, R.J.; Thomas, G.S. The tasselled cap–a graphic description of the spectral-temporal development of agricultural crops as seen by Landsat. In *LARS Symposia*; Purdue University: West Lafayette, IN, USA, 1976.
52. Escadafal, R.; Huete, A. Improvement in remote sensing of low vegetation cover in arid regions by correcting vegetation indices for soil "noise"; Etude des propriétés spectrales des sols arides appliquée à l'amélioration des indices de végétation obtenus par télédétection. FAO. *C. R. Acad. Sci.* **1991**, *312*, 1385–1391.
53. Goel, N.S.; Qin, W. Influences of canopy architecture on relationships between various vegetation indices and LAI and Fpar: A computer simulation. *Remote Sens. Rev.* **1994**, *10*, 309–347. [CrossRef]
54. Huete, A.; Justice, C.; Liu, H. Development of vegetation and soil indices for MODIS-EOS. *Remote Sens. Environ.* **1994**, *49*, 224–234. [CrossRef]
55. Rapinel, S. *Contribution de la Télédétection à l'évaluation des Fonctions des Zones Humides: De l'Observation à la Modélisation Prospective*; Histoire; Université Rennes 2: Rennes, France, 2012.
56. Huete, A.; Jackson, R. Soil and atmosphere influences on the spectra of partial canopies. *Remote Sens. Environ.* **1988**, *25*, 89–105. [CrossRef]
57. Dehouck, A.; Lafon, V.; Lubac, B.; Kervella, S.; Bru, D.; Schmeltz, M.; Roubache, A. Hyperspectral field database in support to coastal wetland mapping. In Proceedings of the 2012 IEEE International Geoscience and Remote Sensing Symposium, Munich, Germany, 22–27 July 2012; pp. 2649–2652. [CrossRef]
58. Lillesand, M.T.; Kiefer, R. *Remote Sensing and Image Interpretation*, 4th ed.; John Wiley and Sons: New York, NY, USA, 2000; 736p.
59. Barillé, L.; Robin, M.; Harin, N.; Bargain, A.; Launeau, P. Increase in seagrass distribution at Bourgneuf Bay (France) detected by spatial remote sensing. *Aquat. Bot.* **2010**, *92*, 185–194. [CrossRef]
60. Bargain, A.; Robin, M.; Meleder, V.; Rosa, P.; Le Menn, E.; Harin, N.; Barille, L. Seasonal spectral variation of Zostera noltii and its influence on pigment-based Vegetation Indices. *J. Exp. Mar. Biol. Ecol.* **2013**, *446*, 86–94. [CrossRef]
61. Dakki, M.; Benhoussa, A.; Hammada, S.; Ibn Tattou, M.; Qninba, A.; El Agbani, M.A. *Cartographie des Habitats Naturels et de la Végétation de Merja Zerga, Maroc. Rapp*; Inédit, MedWet 2; Bureau Ramsar/Administration des Eaux & Forêts et de la Conservation du sol: Dakar, Senegal, 1998.
62. Elso, M.Z.; Manent, P.; Luque, A.; Ramdani, M.; Robaina, R. Genetic Description and Remote Sensing Techniques as Management Tools for Zostera noltii Seagrass Populations along the Atlantic Moroccan Coast. *J. Coast. Res.* **2017**, *33*, 78–87. [CrossRef]
63. Qninba, A.; Benhoussa, A.; El Agbani, M.-A.; Dakki, M.; Thevenot, M. Etude phénologique et variabilité interannuelle d'abondance des Charadriidés (Aves, Charadrii) dans un site Ramsar du Maroc: La Merja Zerga. *Bull. l'Institut Sci.-Fique* **2006**, *28*, 35–47.
64. McKenzie, L.J.; Finkbeiner, M.A.; Kirkman, H. Methods for mapping seagrass distribution. In *Global Seagrass Research Methods*; Elsevier Science B.V: Amsterdam, The Netherlands, 2001; Volume 33, pp. 101–121.
65. Andrade, F.; Ferreira, M.A. A method for monitoring shallow seagrass meadows (*Zostera* spp.) using terrestrial oblique large-scale photography. *Aquat. Bot.* **2011**, *95*, 103–109. [CrossRef]

66. Calleja, F.; Galván, C.; Silió-Calzada, A.; Juanes, J.A.; Ondiviela, B. Long-term analysis of Zostera noltei: A retrospective approach for understanding seagrasses' dynamics. *Mar. Environ. Res.* **2017**, *130*, 93–105. [CrossRef]
67. Kohlus, J.; Stelzer, K.; Müller, G.; Smollich, S. Mapping seagrass (Zostera) by remote sensing in the Schleswig-Holstein Wadden Sea. *Estuar. Coast. Shelf Sci.* **2020**, *238*, 106699. [CrossRef]
68. Traganos, D.; Reinartz, P. Interannual Change Detection of Mediterranean Seagrasses Using RapidEye Image Time Series. *Front. Plant Sci.* **2018**, *9*, 96. [CrossRef]
69. Zhang, C. Applying data fusion techniques for benthic habitat mapping and monitoring in a coral reef ecosystem. *ISPRS J. Photogramm. Remote Sens.* **2015**, *104*, 213–223. [CrossRef]
70. Traganos, D.; Reinartz, P. Mapping Mediterranean seagrasses with Sentinel-2 imagery. *Mar. Pollut. Bull.* **2018**, *134*, 197–209. [CrossRef]
71. Zhang, C.; Selch, D.; Xie, Z.; Roberts, C.; Cooper, H.; Chen, G. Object-based benthic habitat mapping in the Florida Keys from hyperspectral imagery. *Estuar. Coast. Shelf Sci.* **2013**, *134*, 88–97. [CrossRef]
72. Gam, M.; Bazairi, H.; De Montaudouin, X. Impact de la présence d'herbiers à Zostera noltii sur l'infestation parasitaire des coques Cerastoderma edule dans la lagune de Merja Zerga (Maroc). *Bull. l'Institut Sci.* **2009**, *31*, 13–20.
73. Grignon-Dubois, M.; Rezzonico, B. Phenolic chemistry of the seagrass Zostera noltei Hornem. Part 1: First evidence of three infraspecific flavonoid chemotypes in three distinctive geographical regions. *Phytochemistry* **2018**, *146*, 91–101. [CrossRef] [PubMed]
74. Natij, L.; Khalil, K.; Loudiki, M.; Elkalay, K. A first attempt at seagrass repartitioning in the Moroccan coasts. *Int. J. Innov. Sci.* **2014**, *10*, 2351–8014.
75. Touhami, F.; Bazairi, H.; Badaoui, B.; Bouarour, O.; Benhoussa, A. Merja Zerga lagoon: Study of the functional structure and bioassessment of the ecological quality of benthic communities. *J. Mater. Environ. Sci.* **2017**, *8*, 4591–4599. [CrossRef]
76. Touhami, F.; Bazairi, H.; Badaoui, B.; Benhoussa, A. Vertical Distribution of Benthic Macrofauna in Intertidal Habitats Frequented by Shorebirds at Merja Zerga Lagoon. *Thalass. Int. J. Mar. Sci.* **2017**, *34*, 255–265. [CrossRef]
77. Proença, B.; Frappart, F.; Lubac, B.; Marieu, V.; Ygorra, B.; Bombrun, L.; Michalet, R.; Sottolichio, A. Potential of High-Resolution Pléiades Imagery to Monitor Salt Marsh Evolution After Spartina Invasion. *Remote Sens.* **2019**, *11*, 968. [CrossRef]
78. Valle, M.; Palà, V.; Lafon, V.; Dehouck, A.; Garmendia, J.M.; Borja, Á.; Chust, G. Mapping estuarine habitats using airborne hyperspectral imagery, with special focus on seagrass meadows. *Estuar. Coast. Shelf Sci.* **2015**, *164*, 433–442. [CrossRef]
79. Tulldahl, H.M.; Wikström, S.A. Classification of aquatic macrovegetation and substrates with airborne lidar. *Remote Sens. Environ.* **2012**, *121*, 347–357. [CrossRef]
80. Pan, Z.; Fernandez-Diaz, J.C.; Glennie, C.L.; Starek, M. Shallow water seagrass observed by high resolution full waveform bathymetric LiDAR. In Proceedings of the 2014 IEEE Geoscience and Remote Sensing Symposium, Quebec City, QC, Canada, 13 June 2017.
81. Zavalas, R.; Ierodiaconou, D.; Ryan, D.; Rattray, A.; Monk, J. Habitat Classification of Temperate Marine Macroalgal Communities Using Bathymetric LiDAR. *Remote Sens.* **2014**, *6*, 2154–2175. [CrossRef]
82. Ishiguro, S.; Yamada, K.; Yamakita, T.; Yamano, H.; Oguma, H.; Matsunaga, T. Classification of Seagrass Beds by Coupling Airborne LiDAR Bathymetry Data and Digital Aerial Photographs. In *CO_2, Temperature, and Trees*; Springer: Singapore, 2016; pp. 59–70.
83. Parrish, C.E.; Dijkstra, J.A.; O'Neil-Dunne, J.P.M.; McKenna, L.; Pe'eri, S. Post-Sandy benthic habitat mapping using new topobathymetric lidar technology and object-based image classification. *J. Coast. Res.* **2016**, *76*, 200–208. [CrossRef]
84. Webster, T.; McGuigan, K.; Crowell, N.; Collins, K.; Macdonald, C. Optimization of Data Collection and Refinement of Post-processing Techniques for Maritime Canada's First Shallow Water Topographic-bathymetric Lidar Survey. *J. Coast. Res.* **2016**, *76*, 31–43. [CrossRef]
85. Webster, T. Results from 3 seasons of surveys in maritime Canada using the Leica Chiroptera II shallow water topo-bathymetric lidar sensor. In Proceedings of the OCEANS 2017, Aberdeen, UK, 19–22 June 2017; pp. 1–4. [CrossRef]
86. Collings, S.; Campbell, N.A.; Keesing, J.K. Quantifying the discriminatory power of remote sensing technologies for benthic habitat mapping. *Int. J. Remote Sens.* **2018**, *40*, 2717–2738. [CrossRef]
87. Dierssen, H.M.; Zimmerman, R.C.; Leathers, R.A.; Downes, T.V.; Davis, C.O. Ocean color remote sensing of seagrass and bathymetry in the Bahamas Banks by high-resolution airborne imagery. *Limnol. Oceanogr.* **2003**, *48*, 444–455. [CrossRef]
88. Garcia, R.A.; Hedley, J.D.; Tin, H.C.; Fearns, P.R.C.S. A Method to Analyze the Potential of Optical Remote Sensing for Benthic Habitat Mapping. *Remote Sens.* **2015**, *7*, 13157–13189. [CrossRef]
89. Pan, Z.; Glennie, C.; Diaz, J.C.F.; Starek, M. Comparison of bathymetry and sea- grass mapping with hyperspectral imagery and airborne bathymetric lidar in a shallow estuarine environment. *Int. J. Remote Sens.* **2016**, *37*, 516–536. [CrossRef]
90. Castillo-López, E.; Dominguez, J.A.; Pereda, R.; De Luis, J.M.; Pérez, R.; Piña, F. The importance of atmospheric correction for airborne hyperspectral remote sensing of shallow waters: Application to depth estimation. *Atmos. Meas. Tech.* **2017**, *10*, 3919–3929. [CrossRef]
91. Frederiksen, M.; Krause-Jensen, D.; Holmer, M.; Laursen, J.S. Spatial and temporal variation in eelgrass (Zostera marina) landscapes: Influence of physical setting. *Aquat. Bot.* **2004**, *78*, 147–165. [CrossRef]
92. Lathrop, R.G.; Montesano, P.; Haag, S. A Multi-scale Segmentation Approach to Mapping Seagrass Habitats Using Airborne Digital Camera Imagery. *Photogramm. Eng. Remote Sens.* **2006**, *72*, 665–675. [CrossRef]

93. Fletcher, R.S.; Pulich, W.; Hardegree, B. A Semiautomated Approach for Monitoring Landscape Changes in Texas Seagrass Beds from Aerial Photography. *J. Coast. Res.* **2009**, *252*, 500–506. [CrossRef]
94. Young, D.R.; Clinton, P.J.; Specht, D.T. Mapping intertidal eelgrass (*Zostera marina* L.) in three coastal estuaries of the Pa-cific Northwest USA using false colour near-infrared aerial photography. *Int. J. Remote Sens.* **2010**, *31*, 1699–1715. [CrossRef]
95. Uhrin, A.V.; Townsend, P.A. Improved seagrass mapping using linear spectral unmixing of aerial photographs. *Estuar. Coast. Shelf Sci.* **2016**, *171*, 11–22. [CrossRef]
96. Gullström, M.; Lundén, B.; Bodin, M.; Kangwe, J.; Öhman, M.C.; Mtolera, M.S.; Björk, M. Assessment of changes in the seagrass-dominated submerged vegetation of tropical Chwaka Bay (Zanzibar) using satellite remote sensing. *Estuar. Coast. Shelf Sci.* **2006**, *67*, 399–408. [CrossRef]